NEW SIMULATIONS OF POSITRON-BEAM ELECTRON CLOUD BUILD-UP AND ELECTRON-BEAM COUPLED-BUNCH INSTABILITIES FOR KEKB AND SUPER-KEKB

F. Zimmermann*, 31. October 2003

Abstract

I summarize recent electron-cloud and coupled-bunch instability simulation studies for KEKB and Super-KEKB. The possible suppression of the electron-cloud build up inside quadrupole magnets by means of 4 permanent dipoles or by a super-imposed solenoid is investigated for the LER positron beam. Also studied is the electron accumulation in three different types of solenoidal fields, namely for a uniform field and for a series of short separated solenoids with either equal or alternating polarity, considering 4, 2, and 1 rf bucket spacing. No evidence for a 'resonant' build up is found. Simulations for solenoid fields in the Super KEKB upgrade are discussed next. The effective residual electron density in the present KEKB can be estimated from the measured persistent tune shift along the train. The interplay of electron-cloud wake and pinch with the beam-beam interaction in KEKB is studied by a few-particle model, which reveals a potentially large synergy. The vertical coupled-bunch instability growth rate of the HER electron beam is calculated analytically for the resistive-wall impedance and it is found to be a factor 3 smaller than observed. Electron-beam multi-bunch instabilities driven by either resistive-wall or CO ions are also explored in simulations. In the latter case, the effects of a feedback and of beam intensity changes on the growth rates and on the mode spectrum are also investigated. Except for the vertical growth rate, the simulation results may be compatible with observations.

1 INTRODUCTION

During a rather short stay at KEK, from October 27 to November 1, 2003, I resumed simulation studies of the electron-cloud problem for the positron beam and of coupled-bunch instabilities in the HER electron ring.

There is still a persistent electron cloud in KEKB, which is evidenced by the measured tune shift along the train and by variations of the specific luminosity with the bunch spacing. I investigate the possibility that the residual electrons may be trapped in the quadrupole fields, and I explore whether the build up here could be suppressed by either placing permanent dipoles between the quadrupole poles or by superimposing a weak solenoid field on the quadrupole. A simplified solution of the Vlasov equation by A. Novokhatsky and simulations by Y. Cai, M. Pivi, and M. Furman predict a strong resonance dependence of the electron density on the solenoid field. This resonant behaviour has not been observed in KEKB. Below I discuss, if there is any evidence for such a resonance in simulations by the code ECLOUD. Simulations are performed both for the present KEKB and for upgrades with shorter bunch spacing. The magnitude of the residual cloud density can be estimated from the observed tune shift [1]. Using this density value, head-tail instability growth rates for the combined effect of electron cloud and beam-beam interaction can be inferred as a function of the beam-beam tune shift from an analytical 3&4 particle model [2].

In two previous visits I studied the multi-bunch instabilities in the HER using a roughly modelled computer simulation [3]. Meanwhile the experimental growth rates have changed and additional measurements were taken, in particular illuminating the effect of intensity changes and the role of the feedback. One remaining puzzle is that a horizontal instability is seen roughly at the simulated frequency for CO ions, but that a corresponding instability in the vertical plane is not observed. For the purpose of comparison I performed simulations of ion-driven instabilities at different beam intensities and with or without the multi-bunch feedback system. Also the resistive-wall instability was simulated one more time, corroborating a perceived discrepancy between expected and observed growth rates. Simulated growth rates and mode spectra are presented for the two transverse planes.

2 ELECTRON CLOUD

2.1 Field-Free Region

Table 1 lists the parameters assumed for simulations of electron-cloud build up in the LER. Bunch spacings of either 2 or 4 rf buckets (S_b=1.2 or 2.4 m) are considered, with a bunch population N_b of $8\text{x}10^{10}$. The primary photo-electrons are created at a fairly high rate, 0.l5 per meter and second, since there is no antechamber. The reflected photons are taken as distributed according to a $\cos\phi$ distribution, where the angle ϕ is subtended at the point of primary impact. For the elastic electron reflection the parametrization by Hilleret [4] is used. The secondary electron emission is characterized by an intermediate value for the maximum yield at perpendicular incidence of δ_{max}=1.5, with a corresponding primary-electron energy ε_{max} of 200 eV.

Figure 1 shows the simulated evolution of the electron line density for a field-free region and a bunch spacing of 2 rf buckets (4 ns). After about 20 bunch passages, it

*visiting from CERN

saturates around 5-6x10^{10} electrons per meter, close to the neutralization limit N_b/S_b~7x10^{10} m^{-1}. The associated volume density in the vicinity of the beam is displayed in Fig. 2. It peaks near 2x10^{13} m^{-3}, 2 times above the value expected for a uniform distribution.
Figures 3 and 4 show the simulated electron line and volume densities for a bunch spacing of 4 rf buckets. Their saturation values are roughly a factor 2 lower than for the 2-bucket spacing, while the saturation is reached after about half the number of bunches (10 as compared with 20).

Table 1: Parameters for simulations of electron-cloud build up in the LER.

max. sec. emission yield δ_{max}	1.5
(round) half aperture	47 mm
rms horizontal beam size	600 μm
rms vertical beam size	60 μm
rms bunch length	4 mm
bunch population N_b	8x10^{10}
elastic photon reflection	20%
energy of max. sec. yield ε_{max}	200 eV
bunch spacing	1.2, 2.4 m
quadrupole gradient, length	5 T/m, 46 cm
primary e- rate	0.15/e+/m

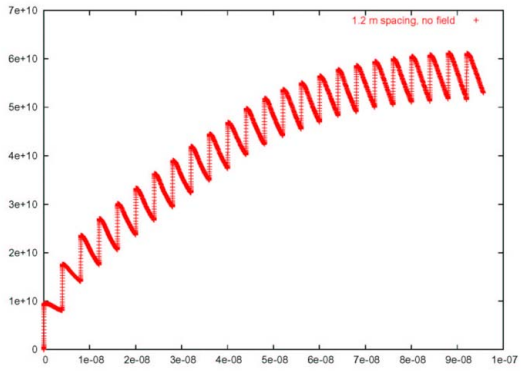

Figure 1: Simulated electron line density for a field-free region, a bunch population of N_b=8x10^{10} and 2 rf bucket spacing.

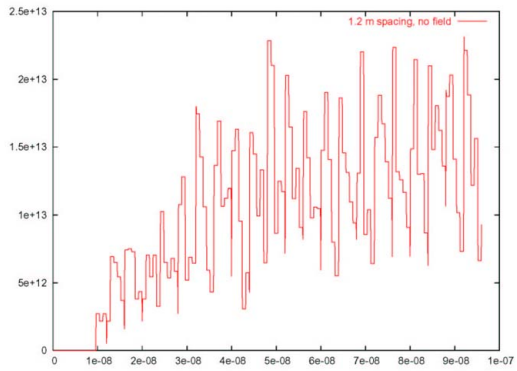

Figure 2: Simulated central volume density for a field-free region, a bunch population of N_b=8x10^{10} and 2 rf bucket spacing.

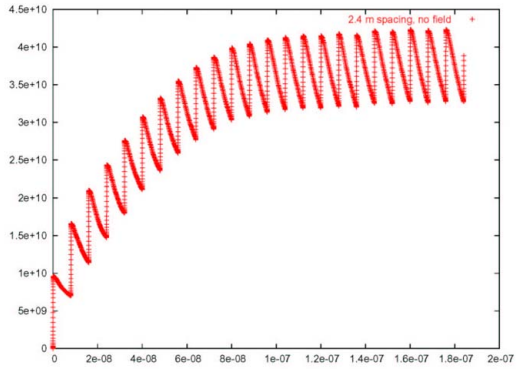

Figure 3: Simulated electron line density for a field-free region, a bunch population of N_b=8x10^{10} and 4 rf bucket spacing.

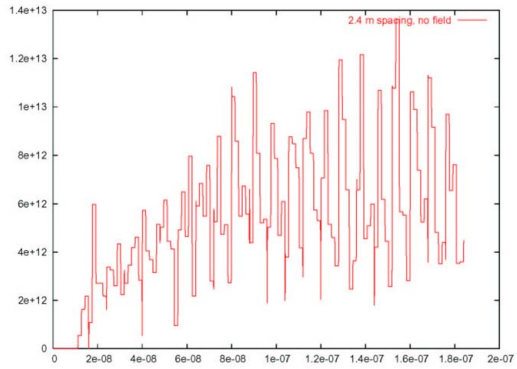

Figure 4: Simulated central volume density for a field-free region, a bunch population of N_b=8x10^{10} and 4 rf bucket spacing.

2.2 Quadrupole Field

The simulated increase of the electron line density inside an LER quadrupole magnet is displayed in Fig. 5 for a bunch spacing of 2 rf buckets. The line density saturates at 3-3.5x10^{10} m^{-1}, which is roughly half the value that is reached without any field (see Fig. 1). The build-up time of 30-40 bunches is almost 2 times longer than in the field-free case. However, while the line density is lower, the central volume density near the beam, about 2x10^{13} m^{-3} as shown in Fig. 6, is comparable to - or even slightly higher than - in the case without magnetic field (Fig. 2). The accumulation of electrons around the beam for a quadrupole field at this bunch spacing is also evident from the snapshot of the macro-electron distribution at the end of the simulation in Fig. 7.

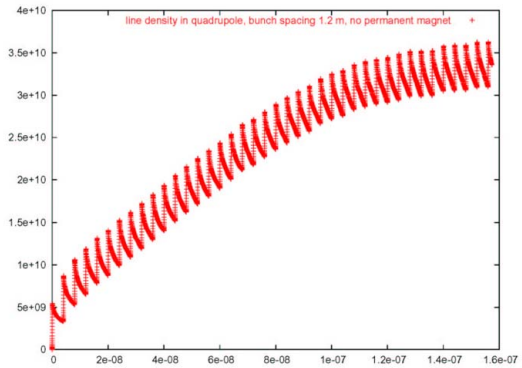

Figure 5: Simulated electron line density for a quadrupole magnet for a bunch population of N_b=8x10^{10} and 2 rf bucket spacing.

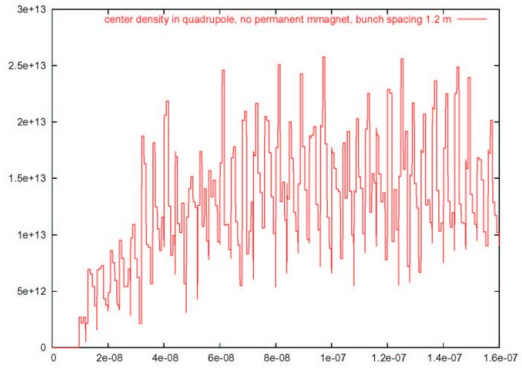

Figure 6: Simulated electron volume density at the center of the vacuum chamber inside a LER quadrupole for a bunch population of 8e10 and a bunch spacing of 2 rf buckets.

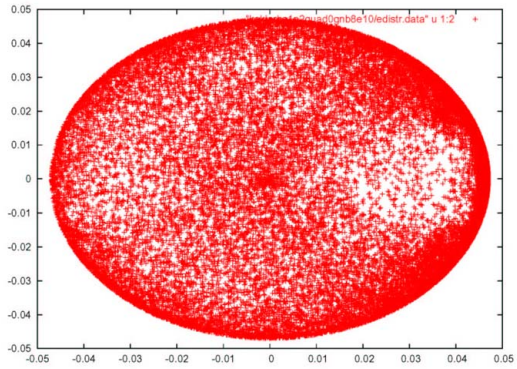

Figure 7: Simulated electron macro-particle distribution after 40 bunch passages for a LER quadrupole field with 2 rf bucket spacing and Nb=8e10.

If we double the bunch spacing to 4 rf buckets, the line density for the quadrupole, in Fig. 8, is again 2 times lower and the build-up time 2 times longer than without field (Fig. 3). It is interesting that, as illustrated in Fig. 9, for this bunch spacing the central volume density remains an order of magnitude below that for a field-free region (Fig. 4).
Hence, there seems to be a threshold in the bunch spacing, below which a large number of electrons may accumulate at the center of the quadrupoles.

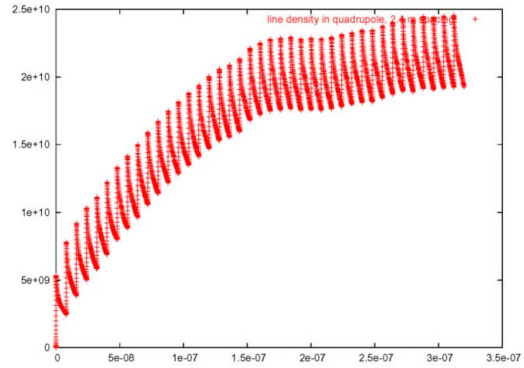

Figure 8: Simulated electron line density for a quadrupole magnet for a bunch population of Nb=8e10 and 4 rf bucket spacing.

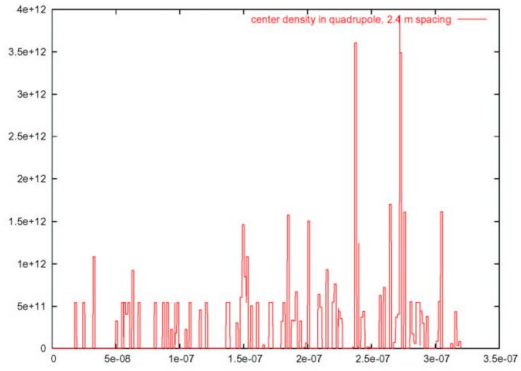

Figure 9: Simulated electron volume density at the center of the vacuum chamber inside a LER quadrupole for a bunch population of 8e10 and a bunch spacing of 4 rf buckets.

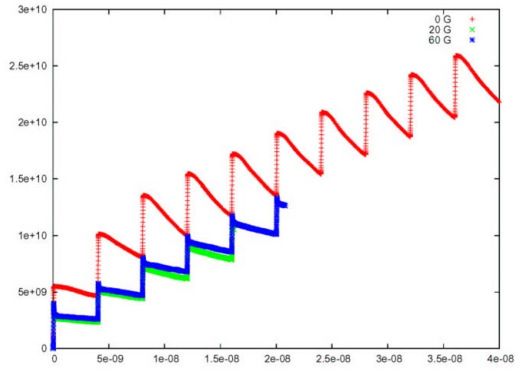

Figure 10: Simulated electron line density as a function of time in seconds for a pure quadrupole field (top curve, red), and with additional permanent dipoles yielding a longitudinal field of 20 G or 60 G at the center between their two poles (the two bottom curves, green and blue), for a bunch spacing of 2 rf buckets.

2.3 Suppression of Electron Build-Up in Quadrupoles by Permanent Dipoles or Solenoids

It has been suggested by H. Fukuma and K. Oide, that the build up of electrons inside the quadrupoles could be suppressed by inserting permanent dipoles between the magnet poles or by super-imposing a solenoid field.
The following simulations address these two possibilities. We model the permanent magnets placed inside a quadrupole crudely as 4 pairs of magnetic monopoles, with their north pole on one longitudinal end of the quadrupole and their south pole at the other end. The strength of these monopoles is chosen such that the field of one pair halfway between its two poles is either 20 G or 60 G. This parametrization introduces a singularity near the monopoles, which we suppress by adding a cut-off parameter at a distance of 1 mm, which might represent the width of the permanent dipole. The chosen configuration generates a non-uniform longitudinal magnetic field along the length of the magnet. Figures 10 and 11 depict the evolution of the simulated electron line density with effective permanent-magnet fields of 0 G, 20 G an 60 G, for a bunch spacing of 2 and 4 rf buckets, respectively. When the permanent magnets are included, the line density at the start of a bunch passage is almost the same as (for 2 rf bucket spacing) or even higher than that for a pure quadrupole field. In addition, the decay time of the electrons is markedly enhanced by the permanent dipoles. The permanent dipoles reduce the central volume density of electrons (not shown) during these first few bunch passages, but a longer-term increase and possible 'trapping' of electrons in the beam vicinity appear likely for this magnet configuration.

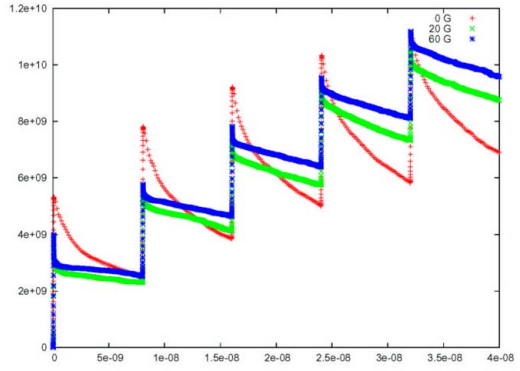

Figure 11: Simulated electron line density as a function of time in seconds for a pure quadrupole field (top curve, red), and with additional permanent dipoles yielding a longitudinal field of 20 G or 60 G at the center between their two poles (the two bottom curves, green and blue), for a bunch spacing of 4 rf buckets.

A superimposed uniform solenoid field is more effective in suppressing the increase of the electron line density inside a quadrupole. This is illustrated in Figs. 12 and 13 for the two bunch spacings. The curves for magnetic fields of 20 G and 60 G are identical. The impact of the solenoid is stronger for the shorter spacing, in Fig. 12, though in the long term the line density may approach a saturation value similar to the case without the solenoid field. Again, the central volume density is also reduced (no significant fraction of macro-electrons reaches the center on the time scale of this simulation), but the steady-state is not yet established, and it thus is hard to draw a definite conclusion on the beneficial effect for a long bunch train. Regardless, the results with a super-imposed uniform solenoid in Figs. 12 and 13 do look

more promising than those for the added permanent dipoles in Figs. 10 and 11.

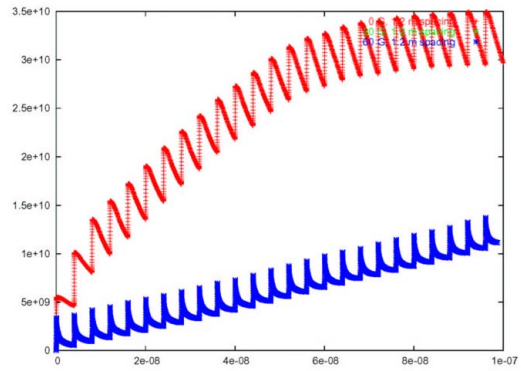

Figure 12: Simulated electron line density as a function of time in seconds for a pure quadrupole field (top curve, red), and with a superimposed uniform solenoid of either 20 G or 60 G (bottom curves - identical), for a bunch spacing of 2 rf buckets.

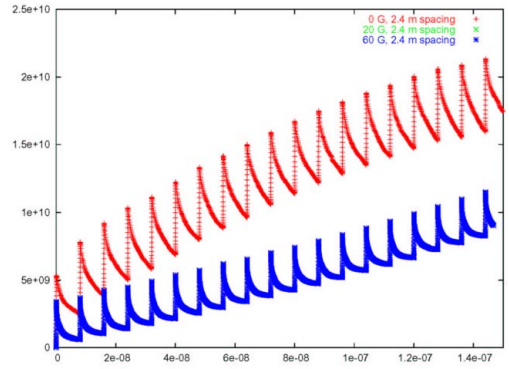

Figure 13: Simulated electron line density as a function of time in seconds for a pure quadrupole field (top curve, red), and with a superimposed uniform solenoid of either 20 G or 60 G (bottom curves - identical), for a bunch spacing of 4 rf buckets.

2.4 Cyclotron Resonance

A. Novokhatsky, Y. Cai et al. have found that the electron build up inside a uniform solenoid should strongly depend on the strength of the solenoid, with maximum electron densities reached for magnetic fields slightly above the 'multipacting resonance':

$$B^c = \frac{\pi mc^2}{eS_b c} \approx \begin{cases} 45\,\mathrm{G} \text{ for } S_b = 1.2\,\mathrm{m} \\ 22\,\mathrm{G} \text{ for } S_b = 2.4\,\mathrm{m} \end{cases}$$

We have explored, if we can find such a resonant dependence in simulations using the ECLOUD code for a typical KEKB LER parameter set, as listed in Table 1 (without quadrupole field). Figure 14 shows the simulated line density for six different solenoid strengths (varying from 10 G to 60 G in steps of 10 G). The line density monotonically decreases with increasing strength of the solenoid. The corresponding volume densities are displayed in Fig. 15. The simulated value is zero for all but the lowest field.

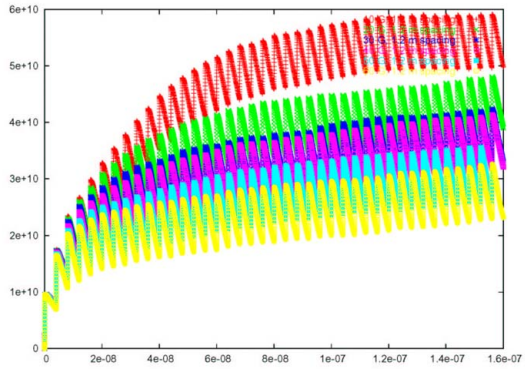

Figure 14: Simulated line density for uniform solenoid fields of strength 10 G, 20 G, 30 G, 40 G, 50 G and 60 G, considering a bunch spacing of 2 rf buckets.

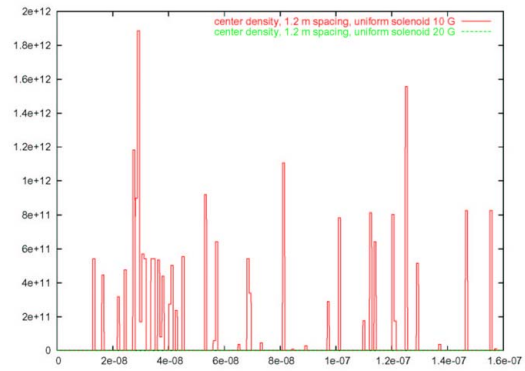

Figure 15: Simulated central volume density for uniform solenoid fields of strength 10 G, 20 G, 30 G, 40 G, 50 G and 60 G, considering a bunch spacing of 2 rf buckets.

The real solenoids are not uniform, but adjacent solenoids, separated by a short gap, can have either equal or opposite polarity. We model the field for an infinite periodic sequence of solenoids with either constant or alternating polarity, using the formula for the solenoid field derived by E. Perevedentsev. We consider a solenoid radius of 70 mm, a solenoid length of 6 mm, and a solenoid spacing of 15 mm. The field strength is scanned from 0 to 60 G.

Figures 16 and 17 display line density and central volume density for the opposite-polarity configuration, Figs. 18 and 19 those for equal polarity. The bunch spacing is 2 rf buckets in all cases. It is evident that adjacent solenoids of equal polarity are considerably more efficient in

suppressing the electron build up. However, even in this case, the build up is not completely extinguished and, in Fig. 18, there is an indication for a slow long-term increase, even for the highest field of 60 G. The slow accumulation of electrons is also present for a uniform field in Fig. 14.

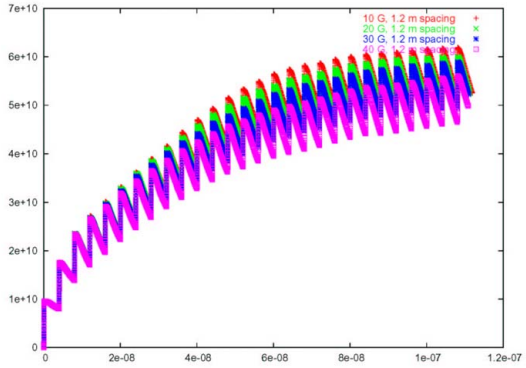

Figure 16: Simulated line density for a series of adjacent solenoids of opposite polarity with strengths 10 G, 20 G, 30 G and 40 G, considering a bunch spacing of 2 rf buckets.

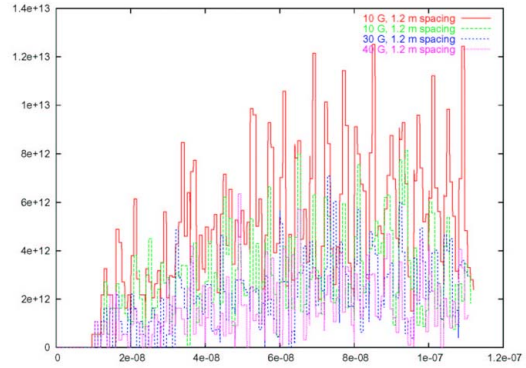

Figure 17: Simulated central volume density for a series of adjacent solenoids of opposite polarity with strengths 10 G, 20 G, 30 G and 40 G, considering a bunch spacing of 2 rf buckets.

2.5 Solenoids for Super-KEKB HER

To take a look at the future, we next examine the electron-cloud build up for a typical parameter set of Super-KEKB, which is summarized in Table 2. The beam pipe is taken to be round with a radius about equal to that of the present LER. The number of primary photo-electrons is, on the one hand, reduced by an antechamber and, on the other hand, increased by the elevated beam energy, assuming that the positrons will be stored in the higher-energy ring. The bunch spacing of 0.6 m corresponds to the filling of every rf bucket. Simulations were performed for two bunch charges, namely either 40% lower or 50% higher than considered earlier for the present and near-term LER.

For the lower charge of 5.2×10^{10} positrons per bunch, the saturated line density simulated with adjacent equal-polarity solenoids of 30 G, in Fig. 20, is about 2 times smaller than that for the present LER with a 40-G field, 2 rf bucket spacing and a bunch population of 8×10^{10}, in Fig. 18. The volume density is displayed in Fig. 21.

For the larger bunch population of 1.2×10^{10}, the line density simulated for adjacent 60-G solenoid fields with equal polarity, in Fig. 22, is comparable to that for the present LER, in Fig. 18, at the field strength of 40 G. The corresponding volume density is shown in Fig. 23.

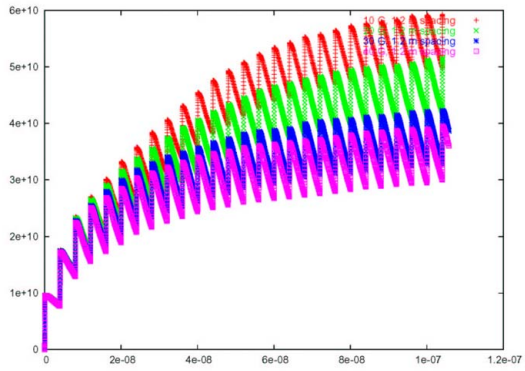

Figure 18: Simulated line density for a series of adjacent solenoids of equal polarity with strengths 10 G, 20 G, 30 G and 40 G, considering a bunch spacing of 2 rf buckets.

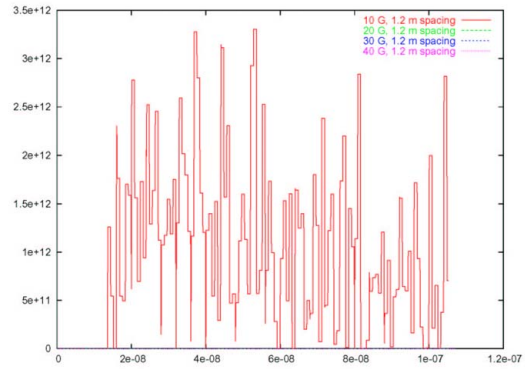

Figure 19: Simulated central volume density for a series of adjacent solenoids of equal polarity with strengths 10 G, 20 G, 30 G and 40 G, considering a bunch spacing of 2 rf buckets.

Table 2 Parameters of electron-cloud simulations for SuperKEKB.

max. sec. emission yield δ_{max}	1.5
(round) half aperture	45 mm
rms horizontal beam size	600 μm
rms vertical beam size	60 μm
rms bunch length	3 mm
bunch population N_b	$5.2\text{x}10^{10}$,$1.2\text{x}10^{11}$
γ absorption in antechamber	90%
energy of max. sec. yield ε_{max}	200 eV
primary e- rate	0.027/e+/m
bunch spacing	0.6 m

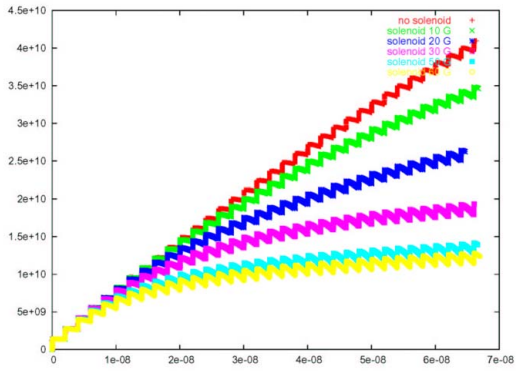

Figure 20: Simulated line density for a series of adjacent solenoids of equal polarity with strengths 0 G, 10 G, 20 G, 30 G, 50 G and 60 G, considering a bunch spacing of 1 rf bucket and $5.2\text{x}10^{10}$ positrons per bunch.

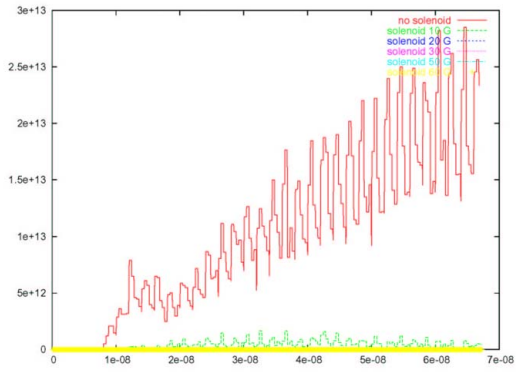

Figure 21: Simulated central volume density for a series of adjacent solenoids of equal polarity with strengths 0 G, 10 G, 20 G, 30 G, 50 G and 60 G, considering a bunch spacing of 1 rf bucket and $5.2\text{x}10^{10}$ positrons per bunch.

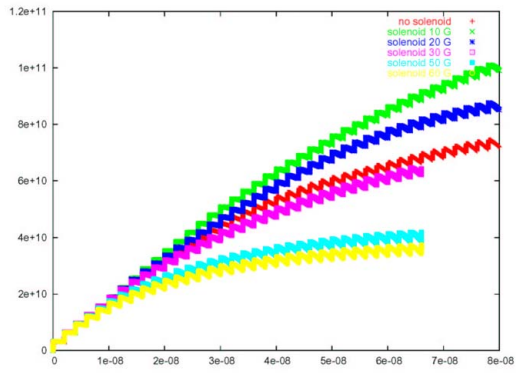

Figure 22: Simulated line density for a series of adjacent solenoids of equal polarity with strengths 0 G, 10 G, 20 G, 30 G, 50 G and 60 G, considering a bunch spacing of 1 rf bucket and $1.2\text{x}10^{11}$ positrons per bunch.

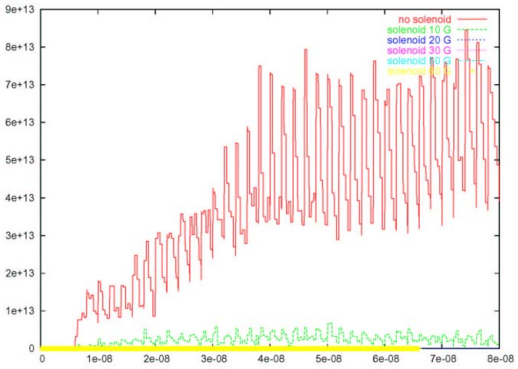

Figure 23: Simulated central volume density for a series of adjacent solenoids of equal polarity with strengths 0 G, 10 G, 20 G, 30 G, 50 G and 60 G, considering a bunch spacing of 1 rf bucket and $1.2\text{x}10^{11}$ positrons per bunch.

2.6 Enhancement of Electron-Cloud Induced Blow-Up by Beam-Beam Tune Shift

The measured specific luminosity for different bunch spacing suggests that the combined effect of electron-cloud and beam-beam interaction is more harmful than the two phenomena individually. This synergy can be modelled in a weak-strong approximation by a few-particle model, where the electron cloud is represented both by a constant wake field coupling leading and trailing particles and by a linear tune shift along the bunch, and the beam-beam interaction is modelled by an inverse parabolic tune variation with longitudinal distance from the bunch centre. The model was described in Ref. [2]. Assuming a net electron density of $6\text{x}10^{11}$ m-3, which is suggested by tune-shift measurements (see below), we can compute the dependence of the head-tail growth rates on the beam-beam parameter for KEKB. The

resulting growth times for the 3 and 4-particle models are shown in Fig. 24. There is still a large difference between the cases of 3 and 4 particles, which indicates a slow convergence. Nevertheless, the curves suggest that the growth times are shorter than 1 ms, and that the beam-beam interaction for the B factory (positive ξ) likely acts destabilizing and possibly reduces the rise time by a factor of 2.

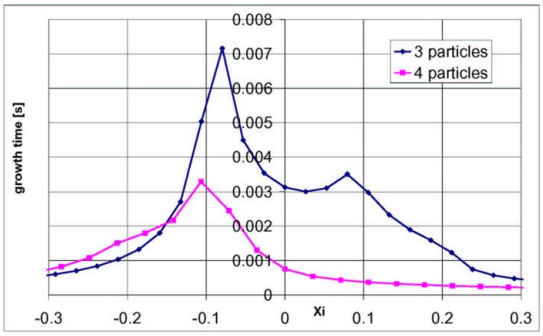

Figure 24: Growth time of the head-tail instability driven by electron cloud and beam-beam interaction for a cloud density of $\rho=6\times10^{10}$ m^{-3} as a function of beam-beam tune shift, according to the 3 and 4-particle models.

It has been criticized that the multi-particle models do not predict a clear instability threshold, unlike the 2-particle model for the conventional head-tail instability. Figure 25 shows the growth rate computed in the 3 and 4-particle models for a regular constant wake field, i.e., without linear and parabolic tune shift representing electron pinch or beam-beam effect. Though the growth rate never is exactly zero, there is an apparent threshold around a wake-field strength of 6-7x10^5 m^{-2}, slightly less than the threshold predicted by the classical 2-particle model:

$$W_{thr,2\,part} \approx \frac{8\gamma C\omega_\beta\omega_s}{\pi r_e c^2 N_b} \approx 8.4\times10^5\,\mathrm{m}^{-2}$$

Therefore, we expect that for practical purposes also the multi-particle model can explain observed 'thresholds'.

2.7 Estimate of Residual Electron Density from Tune Shift

The measured persistent tune shift along the train [1] can be used to estimate the effective net electron volume density as follows,

$$\rho \approx (1...2)\gamma\frac{\Delta\nu}{r_e\oint\beta\,ds} \approx (3...6)\times10^{11}\ \mathrm{m}^{-3}$$

$$\text{for } \oint\beta\,ds \approx 40000\ \mathrm{m}^2 \text{ and } \Delta\nu \approx 0.005$$

Here the factor 2 uncertainty refers to the difference between a 'flat' and 'round' electron-cloud symmetry. The estimated density of 3-6x10^{11}m^{-3} is close to the head-tail instability threshold estimated in early 2001 [7].

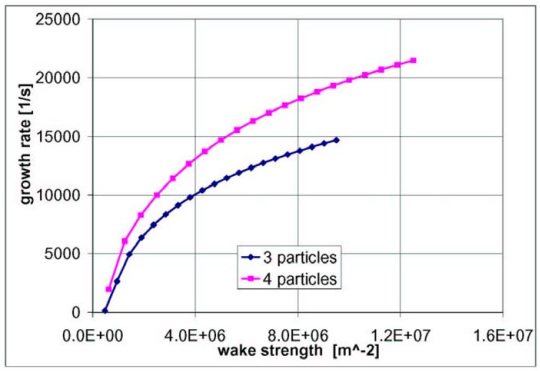

Figure 25: Growth rate of conventional head-tail instability without tune shift from electron pinch and without tune shift due to beam-beam interaction as a function of the head-tail wake strength, predicted by 3 and 4-particle models.

3 HER MULTI-BUNCH INSTABILITIES

3.1 Analytical Estimate for Resistive-Wall Effect

The fastest growing multi-bunch mode for the resistive-wall impedance is found at low frequency, with the mode betatron tune negative and closest to 0. The growth rate of this mode for a round pipe is given by A. Chao [8]. For the elliptical pipe of the HER we need to multiply the round-pipe values with a 'Yokoya' factor [9] of about 0.8 vertically and 0.5 horizontally (the HER chamber has half axes of 52 mm and 28.5 mm, flattened in the vertical direction at a half height of 25 mm). Including the Yokoya factor, the fastest vertical growth rate becomes

$$\frac{1}{\tau_{(\mu)}} \approx -0.8\frac{MNr_0c^2}{b^3\gamma\omega_\beta T_0\sqrt{2\pi\sigma\omega_0}}\frac{\mathrm{sgn}(\Delta_\beta)}{\sqrt{|\Delta_\beta|}}$$

$$M \approx 1152$$

$$N \approx 2.8x10^{10}$$

$$b = 25\ \mathrm{mm}$$

$$\Delta_\beta \approx -0.42,\ \gamma \approx 15660$$

$$\sigma \approx 5.4\times10^{17}\ \mathrm{s}^{-1}\ \text{(Copper)}$$

$$\omega_\beta \approx 41.58\times6.2\times10^5\ \mathrm{s}^{-1}$$

where we have also listed parameters for the KEKB HER during some experimental growth rate measurements. This analytical expression evaluates to a growth time of 9 ms, while the observed value is of the order of 2-3 ms

[10]. This difference may indicate the presence of other impedance sources. A good candidate might be the movable masks, which are placed nearest to the beam. On the other hand, a change in the resistivity of the copper chamber due to heating is not a likely explanation, since for a resistivity temperature coefficient of 0.004/K for copper, a temperature of 2300 K would be needed to account for a factor 3 increase in growth rate. This is about two times the melting point. The horizontal growth time should be 0.8/0.5 times larger than the vertical, so that its analytically predicted value is about 14 ms, if it is driven by the resistive wall of the arc chamber.

3.2 Multi-Bunch Simulations for Resistive Wall

To investigate the above issues further, we have performed a series of multibunch simulations along the lines of Ref. [11]. All multibunch simulations whose results are presented in the following assume a bunch spacing of 4 rf buckets and either 1200 or 1152 consecutive bunches, corresponding to a gap of either 80 or 128 missing bunches, respectively. The vertical betatron tune is taken to be 41.585 and the horizontal tune 44.514. The horizontal and vertical emittances are 24 nm and 0.36 nm, except for the last 4 pictures which approach Super-KEKB, where the vertical emittance is reduced to 0.18 nm. An average beta function of 15 m is considered for both planes and all cases. The nominal bunch population in the simulation is $N_b=3.5x10^{10}$.

Figures 26 and 27 show the simulated horizontal and vertical positions, respectively, of bunches 500 and 1000 in a train of 1200 at a single location over 512 turns. Figures 28 and 29 show the corresponding frequency spectra, as computed from the positions of all bunches recorded over 512 turns. As expected they peak at low frequencies, and the lower betatron sidebands are more pronounced than the upper ones.

Horizontal position and spectra for 2048 turns are displayed in Figs. 30 and 31. From Fig. 30, we estimate the horizontal growth time to be about 9-16 ms, which appears roughly consistent with the analytical estimate for a uniform fill pattern.

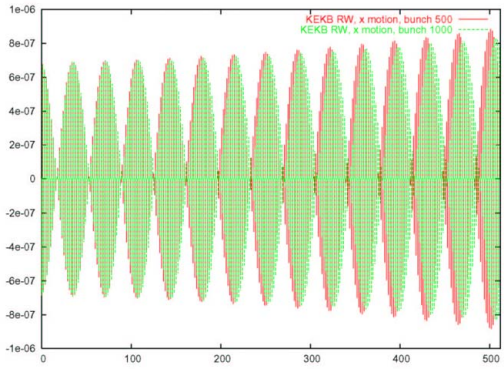

Figure 26: Simulated horizontal position for bunches 500 and 1000 of a 1200-bunch train in the presence of a resistive-wall wake over 512 turns, for $N_b=3.5x10^{10}$.

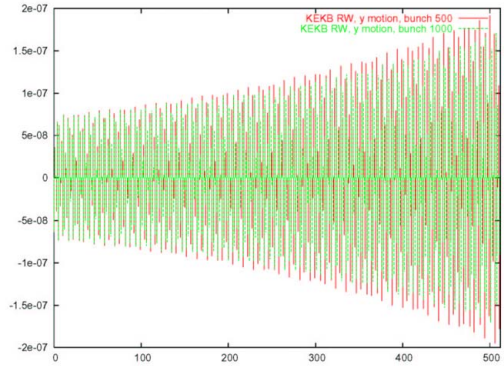

Figure 27: Simulated vertical position for bunches 500 and 1000 of a 1200-bunch train in the presence of a resistive-wall wake over 512 turns, for $N_b=3.5x10^{10}$.

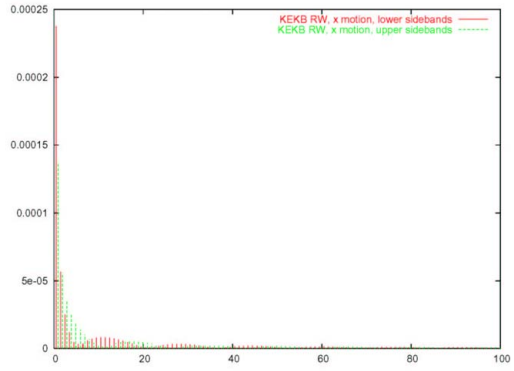

Figure 28: Upper and lower betatron sidebands around the first 100 revolution harmonics in the horizontal plane for the resistive-wall wake field of the HER arc chamber, simulated over 512 turns, for $N_b=3.5x10^{10}$.

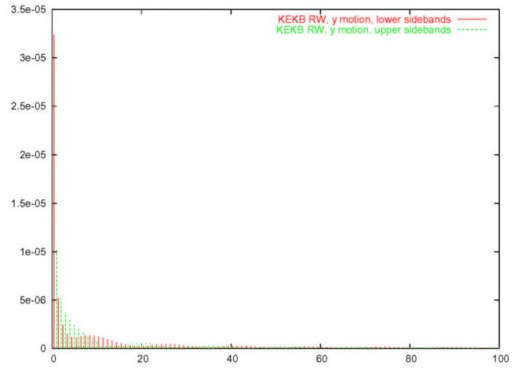

Figure 29: Upper and lower betatron sidebands around the first 100 revolution harmonics in the vertical plane for the resistive-wall wake field of the HER arc chamber, simulated over 512 turns, for N_b=3.5x10^{10}.

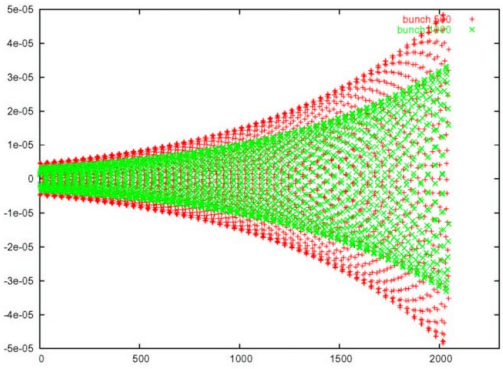

Figure 30: Simulated horizontal position for bunches 500 and 1000 of a 1200-bunch train in the presence of a resistive-wall wake over 2048 turns, for N_b=3.5x10^{10}.

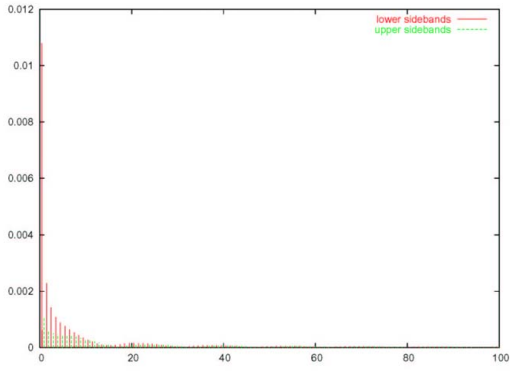

Figure 31: Upper and lower betatron sidebands around the first 100 revolution harmonics in the horizontal plane for the resistive-wall wake field of the HER arc chamber, simulated over 2048 turns, for N_b=3.5x10^{10}.

3.3 Multi-Bunch Simulations for CO Ions without Magnetic Field with or without Feedback and for Various Intensities

We next simulate the effect of CO ions, which in [11] were found to be a likely source for the horizontal instability, based on a comparison of observed and simulated mode spectra and growth rates. To enhance the effect, as in [11] we artificially increase the CO pressure to 10^{-6} Pa in the simulation, while the real pressure is less than 10^{-9} Pa. Figures 32 and 33 show the simulated horizontal and vertical positions, respectively, of bunches 500 and 1000 over 51 turns, and Figs. 34 and 35 present the associated mode spectra.

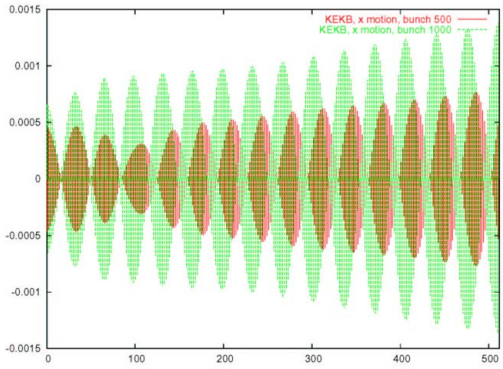

Figure 32: Simulated horizontal position for bunches 500 and 1000 of a 1152-bunch train in the presence of a CO ions at a pressure of 10^{-6} Pa, over 512 turns, for N_b=3.5x10^{10}.

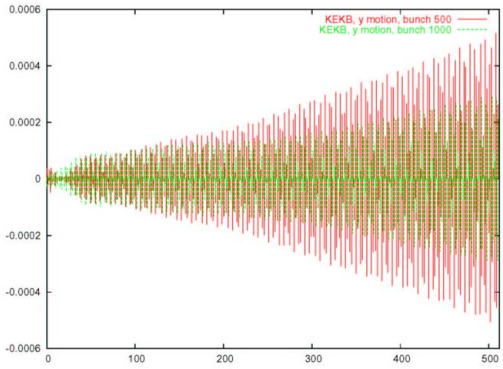

Figure 33: Simulated vertical position for bunches 500 and 1000 of a 1152-bunch train in the presence of a CO ions at a pressure of 10^{-6} Pa, over 512 turns, for N_b=3.5x10^{10}.

Evidently the mode spectra are distinctly different from the resistive-wall case. They peak around integer values of about 15 and 35, in the two planes. Over the 512 turns considered, the oscillation amplitude reaches a maximum of 2σ in the horizontal plane, while it approaches 7σ

vertically. The highly nonlinear force at this amplitude may explain why the simulated ratio of the peak frequencies is about 2.3 instead of 3.2 expected from the beam size.

Experimentally it was observed that the multi-bunch feedback affects the mode spectra [10]. We have repeated the previous simulations including a bunch-by-bunch feedback which acts on the oscillation amplitude of each bunch on each turn. The 'gain' of the feedback was determined as $1/(f_{rev}*\tau_{fdbk})$, where f_{rev} denotes the revolution frequency and τ_{fdbk} the feedback damping time, which we set to 1 ms. The resulting oscillations in the two transverse planes are illustrated in Figs. 36 and 37. The oscillations now stay below 1σ horizontally and below 3σ vertically. The mode spectra for these cases are shown in Figs. 38 and 39. The peak of the horizontal signal near mode 15 is roughly unchanged, but it appears that the effect of the feedback has shifted the centroid of the vertical mode spectrum mode by about a factor of 2 downwards to about 20.

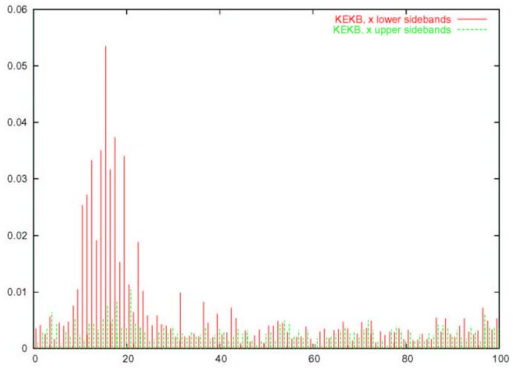

Figure 34: Upper and lower betatron sidebands around the first 100 revolution harmonics in the horizontal plane train for CO ions at a pressure of 10^{-6} Pa, with $N_b=3.5x10^{10}$, simulated over 512 turns.

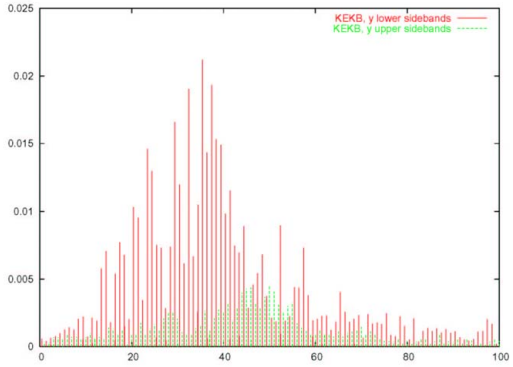

Figure 35: Upper and lower betatron sidebands around the first 100 revolution harmonics in the vertical plane train for CO ions at a pressure of 10^{-6} Pa, with $N_b=3.5x10^{10}$, simulated over 512 turns.

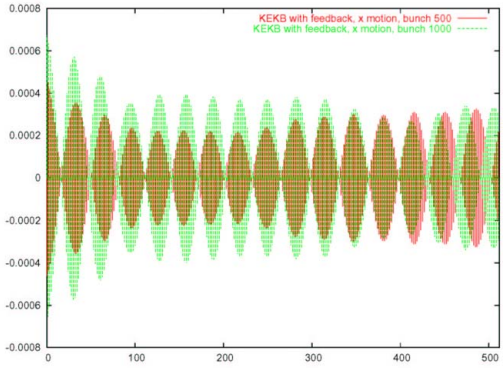

Figure 36: Simulated horizontal position for bunches 500 and 1000 of a 1152-bunch train in the presence of a CO ions at a pressure of 10^{-6} Pa, over 512 turns, for $N_b=3.5x10^{10}$, including a multi-bunch feedback with 1 ms damping time.

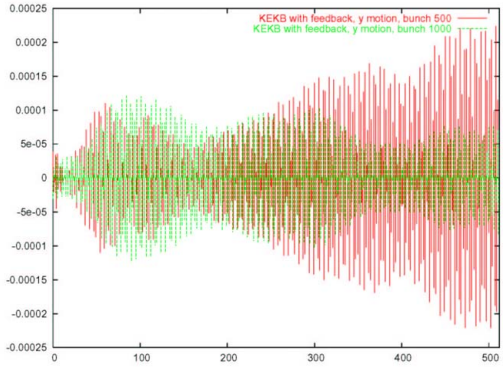

Figure 37: Simulated vertical position for bunches 500 and 1000 of a 1152-bunch train in the presence of a CO ions at a pressure of 10^{-6} Pa, over 512 turns, for $N_b=3.5x10^{10}$, including a multi-bunch feedback with 1 ms damping time.

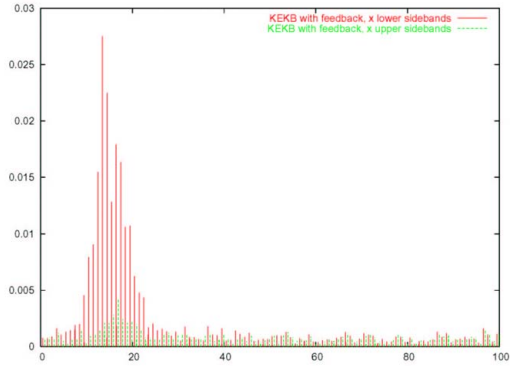

Figure 38: Upper and lower betatron sidebands around the first 100 revolution harmonics in the horizontal plane train for CO ions at 10^{-6} Pa, with $N_b=3.5x10^{10}$ over 512 turns, including a feedback with 1 ms damping time.

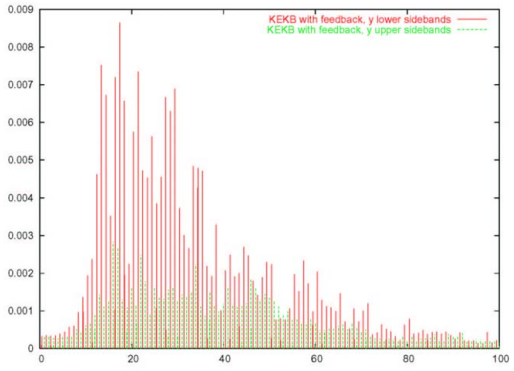

Figure 39: Upper and lower betatron sidebands around the first 100 revolution harmonics in the vertical plane train for CO ions at a pressure of 10^{-6} Pa, with N_b=3.5x10^{10}, simulated over 512 turns, including a multi-bunch feedback with 1 ms damping time.

We finally investigate the dependence on the bunch intensity. First, without any feedback, we reduce the beam current by about 30% to N_b=2.2x10^{10}, with results as shown in Figs. 40-43. These should be compared with Figs. 32-35 for the higher intensity of N_b=3.5x10^{10}. At the lower intensity, the instability has slowed down, saturates horizontally and decreases in growth rate by a factor 2 vertically. The mode spectra are shifted downward by about 10-20%, compatible with the expected dependence.

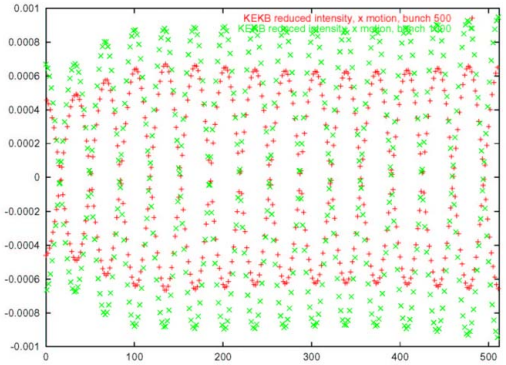

Figure 40: Simulated horizontal position for bunches 500 and 1000 of a 1152-bunch train in the presence of a CO ions at a pressure of 10^{-6} Pa, over 512 turns, for a reduced intensity of N_b=2.2x10^{10}.

Next, we increase the bunch intensity to N_b=1.2x10^{11}, and reduce the vertical emittance by 50% to 180 pm. This approximates the SuperKEKB upgrade. However, we do not change the bunch spacing here, but keep it at 4 rf buckets. The results are summarized in Figs. 44-47. The horizontal motions appears stabilized at this increased intensity, while the vertical growth rate at first looks comparable to the present nominal case (Fig. 33), but then saturates after about 200 turns. The peak of the horizontal mode spectrum has shifted from mode 15 to about 20 and the vertical from 35 to 50. Both shifts are consistent with the change in the bunch charge.

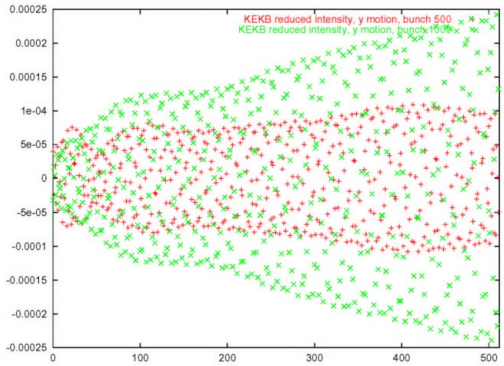

Figure 41: Simulated vertical position for bunches 500 and 1000 of a 1152-bunch train in the presence of a CO ions at a pressure of 10^{-6} Pa, over 512 turns, for a reduced intensity of N_b=2.2x10^{10}.

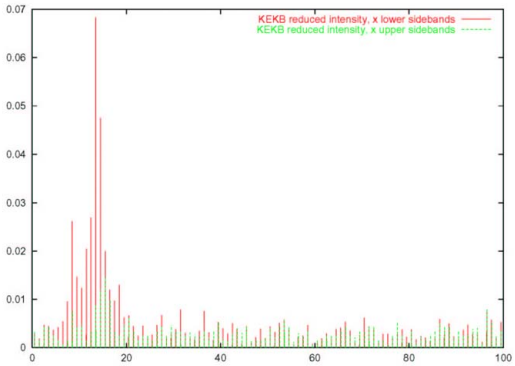

Figure 42: Upper and lower betatron sidebands around the first 100 revolution harmonics in the horizontal plane train for CO ions at a pressure of 1e-6 Pa, with a reduced intensity of Nb=2.2x10^{10}, simulated over 512 turns.

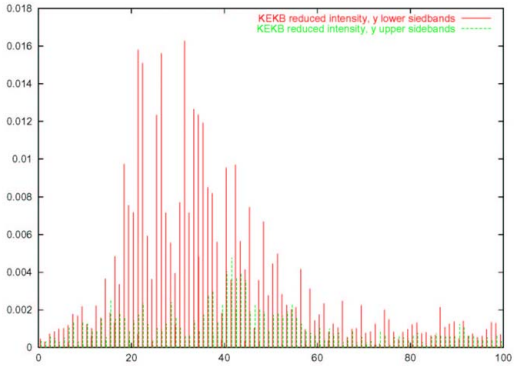

Figure 43: Upper and lower betatron sidebands around the first 100 revolution harmonics in the vertical plane train for CO ions at a pressure of 10^{-6} Pa, with a reduced intensity of N_h=2.2x10^{10}, simulated over 512 turns.

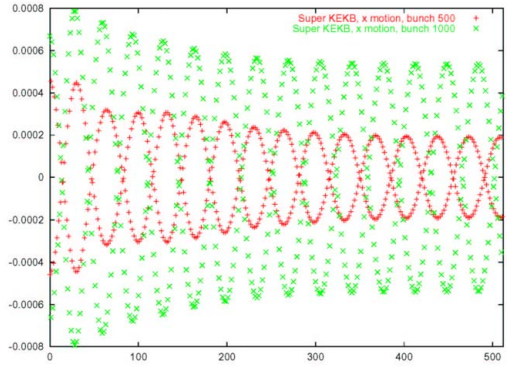

Figure 44: Simulated horizontal position for bunches 500 and 1000 of a 1152-bunch train with 4-bucket spacing in the presence of a CO ions at a pressure of 10^{-6} Pa, over 512 turns, for N_b=1.2x10^{11} and a vertical emittance of 180 pm.

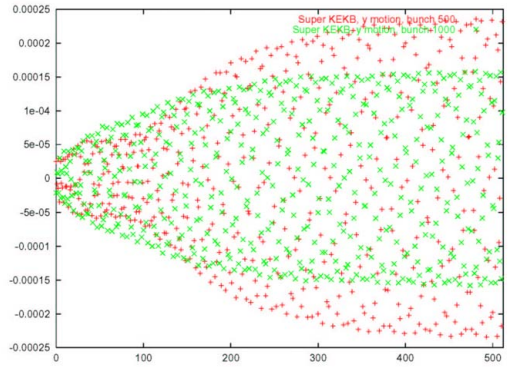

Figure 45: Simulated vertical position for bunches 500 and 1000 of a 1152-bunch train with 4-bucket spacing in the presence of a CO ions at a pressure of 1e-6 Pa, over 512 turns, for Nb=1.2e11 and a vertical emittance of 180 pm.

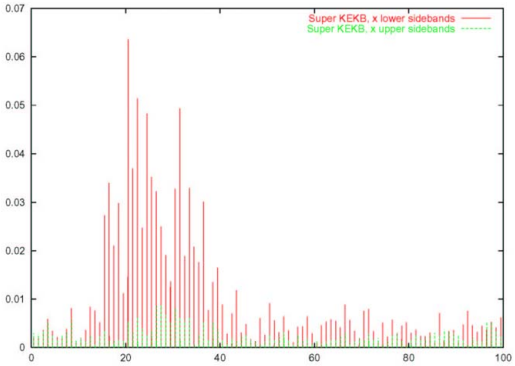

Figure 46: Upper and lower betatron sidebands around the first 100 revolution harmonics in the horizontal plane train for CO ions at a pressure of 1e-6 Pa, for a 1152-bunch train with 4-bucket spacing with Nb=1.2e11, and a vertical emittance of 180 pm, simulated over 512 turns.

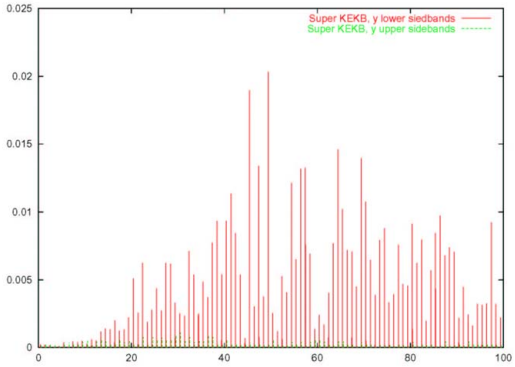

Figure 47: Upper and lower betatron sidebands around the first 100 revolution harmonics in the vertical plane train for CO ions at a pressure of 1e-6 Pa, for a 1152-bunch train with 4-bucket spacing with Nb=1.2e11, and a vertical emittance of 180 pm, simulated over 512 turns

4 OTHER ISSUES

A number of other possible issues for KEKB remain unaddressed due to lack of time or competence, though I would have liked to look into them. These include the possibility of designing a Raimondi-Seryi compact final focus for SuperKEKB [12], the option of colliding long super-bunches [13], the relevance of the CSR instability for the KEKB KER [14], the diurnal variation of the KEKB luminosity [15], and an analytical expression for the self-consistent beam distributions of two beams in collision [16].

Concerning the electron cloud, in the past concerns were raised by S. Olsen and more recently by A. Novokhatsky that photo-electrons could be emitted with keV energies. Measurements by Suetsugu and colleagues did not seem to bear any evidence for a significant high-energy component, however. More informations on this point would be helpful. Simulations with the code HEADTAIL should be conducted for the experimentally inferred and simulated values of cloud-densities (e.g., assuming that the electrons located in a quadrupole field) and using the actual chromaticities.

5 SUMMARY

In the first part of this report, we have investigated the electron cloud build up for fields composed of quadrupoles, solenoids and permanent dipoles. The present electron-cloud build up in the LER with a 40 G solenoid field for 2 rf bucket spacing appears comparable

to that in a SuperKEKB with a 60-G field, antechamber, $1.2x10^{11}$ positrons per bunch, and 1 rf bucket spacing (with equal polarity for adjacent solenoid coils). Electron density at the center of the quadrupole is significant for 2 rf bucket spacing, but small for 4 rf bucket spacing. Permanent dipoles placed between the poles of a quadrupole seem to likely increase the number of electrons in the beam pipe, at least for the present model of the permanent dipoles. On the other hand, a weak solenoid superimposed on the quadrupole might be effective in reducing the electron density. Our simulations provide no strong evidence of the cyclotron resonance for a solenoid field postulated by A. Novokhatsky and J. Seeman, and simulated by Y. Cai and co-workers. Rather we find a monotonic decrease of the electron density with increasing solenoid field. The residual cloud density estimated from the measured tune shift along the bunch train is still close to the threshold of the head-tail instability. A 4-particle model representing the combined effect of beam-beam tune shift, electron pinch, and electron-cloud short-range wake predicts a sub-ms growth rate and potentially a factor of 2 enhancement of the growth rate by the beam-beam interaction.

In the second part, we have studied the multi-bunch instability in the HER. There appears to be a factor 3 discrepancy between the measured and calculated resistive-wall coupled-bunch growth rate in the vertical plane of the HER. The simulated growth rate (with a small gap) is roughly consistent with the analytical estimate for a uniform bunch pattern. The comparison suggests the presence of an unidentified dominant source of resistive-wall impedance driving the vertical instability. The simulated mode spectra for ion-driven instabilities are similar to observations in the horizontal plane. The effect of the feedback may also resemble the measurements. The mode spectra respond to intensity changes as expected. Why no vertical ion instability is observed remains unclear.

Further studies and a better understanding are still needed.

6 ACKNOWLEDGEMENTS

I thank K. Oide for inviting me to KEK, and all KEKB members for the wonderful hospitality. This study greatly profited from discussions with - and help by - H. Fukuma, Y. Funakoshi, H. Koiso, K. Ohmi, and K. Oide.

REFERENCES

[1] H. Fukuma et al., Recent Observations of Collective Effects at KEKB, Presentation at Factories'03, Stanford, Oct. 2003 (2003).

[2] G. Rumolo and F. Zimmermann, Two-Stream Instability Workshop, KEK, Tsukuba 2001 (2001).

[3] F. Zimmermann et al., PAC 2003 Portland Oregon (2003).

[4] V. Baglin, I. Collins, B. Henrist, N. Hilleret, and G. Vorlaufer, A Summary of Main Expperimental Results Concerning the Secondary Electron Emission of Copper, LHC Project Report 472 (2002).

[5] A. Novokhatski, and J. Seeman, Simulation Study of Electron Cloud Multipacting in Straight Sections of PEP-II, PAC2003 Portland Oregon (2003).

[6] Y. Cai, M. Pivi, M.A. Furman, Build Up of Electron Cloud in the PEP-II Particle Accelerator in the Presence of a Solenoid Field and with Different Bunch Pattern, SLAC-PUB-10164 (2003).

[7] K. Ohmi and F. Zimmermann, Head-Tail Instability Caused by Electron Cloud in Positron Storage Rings, Phys. Rev. Lett. 85, 3821 (2000).

[8] A. Chao, Physics of Collective Instabilities in High Energy Accelerators, J. Wiley (1993).

[9] K. Yokoya, Resistive Wall Impedance of Beam Pipes of General Cross Section, Part. Acc. 41, p. 221 (1993).

[10] H. Fukuma, private communication (2003).

[11] F. Zimmermann, H. Fukuma, K. Ohmi, Y. Ohnishi, S.S. Win, Simulation Study of Coupled-Bunch Instabilities due to Resistive Wall, Ions, or Electron Cloud, PAC2003, Portland (2003).

[12] F. Zimmermann, Raimondi-Seryi Final Focus for e+/e- Factories?, Factories'03 Stanford (2003).

[13] F. Zimmermann, Brief Review of Superbunches for Hadron Colliders, Factories'03 Stanford (2003).

[14] G. Stupakov, CSR Effects in e+e- Storage Rings, Factories'03 Stanford (2003).

[15] Y. Funakoshi, Status and Future Plans of KEKB, Factories'03 Stanford (2003).

[16] K. Ohmi, Summary of Beam-Beam Effects, Factories'03 Stanford (2003).